Day-Ahead Optimal Operation for Multi-Energy Residential Systems with Renewables

Weijia Liu, Junpeng Zhan, *Member, IEEE*, C. Y. Chung, *Fellow, IEEE*, and Yang Li

***Abstract* — The intermittency and stochasticity nature of distributed renewable energy sources has introduced great challenges to the efficiency and security of energy distribution system operations. To address the negative impacts of intermittent renewable energy sources, this paper proposes a day-ahead optimal operation strategy utilizing distributed energy resources based on the framework of the interconnected multi-energy system. First, a framework and mathematical models of multi-energy residential systems (MERS) are proposed. Based on the characteristics of residential energy distribution networks, the complex MERS models are reformulated to relieve the computational burden. Furthermore, the uncertainty factors such as renewable energy generation fluctuations and demand variations are handled by a reformulated chance constrained programming technique. The feasibility and effectiveness of the proposed method are validated through a combined electric power and natural gas test system. Compared to similar models and methods in the existing literature, the proposed method performs better in terms of solution time, model scalability, and robustness in handling uncertainties.**

***Index Terms* — Distributed energy resources, energy storage, multi-energy system, renewable energy**

NOMENCLATURE

Sets and Indexes

Ω_H /h	Set and index of residential houses
Ω_K /k	Set and index of combined heat and power unit operational corner points
Ω_T /t	Set and index of time slots
Ω_{CHP}^{n}	Set of houses accessible to the heat production of combined heat and power unit at node n

Parameters

C_h^{in} , C_h^{sf}	Heat capacities of house interior and surface
G_{n-m} , B_{n-m}	Real/imaginary part of the admittance matrix
$H_{n,k}^{CHP}$, $P_{n,k}^{CHP}$, $q_{n,k}^{CHP}$	Corner point heat output, power output and natural gas consumption of combined heat and power unit
$H_{h,t}^{in,rad}$, $H_{h,t}^{sf,rad}$	House interior and surface heat radiation
M	Large positive number
$P_{n,t}^{D,fix}$	Fixed nodal power load
t_{start} , t_{end}	First and last considered time slot
T_t^{ext} , $T_{balance}^{ext}$	Ambient temperature and balance temperature of dual fuel heat pump and gas furnace
n_s , i_s	Electric power and natural gas source node
λ_t^E , λ_t^G	Electricity and natural gas energy price
φ_{i-j} , μ_{i-j}	Natural gas pipeline and linepack diameters
β , η , τ	Polytropic exponent, overall efficiency and fuel rate coefficient of a compressor
η_h^{HP} , η_h^{GF}	Efficiency of heat pump and gas furnace
$\eta^{ES,in}$, $\eta^{ES,out}$	Charge/discharge efficiency of electricity and natural gas storage
$\eta^{GS,in}$, $\eta^{GS,out}$	
γ_h^{HP} , γ_h^{GF}	Identifier of heat pump and gas furnace
ζ_h^{is} , ζ_h^{ie} , ζ_h^{se}	Heat transfer capacities among house interior, surface, and exterior
ϕ_P , ϕ_Q , ϕ_V , ϕ_I , ϕ_λ	Confidence coefficient of chance constraints
$\mathbf{\Psi_P}$, $\mathbf{\Psi_Q}$, $\mathbf{\Psi_V}$, $\mathbf{\Psi_I}$, $\mathbf{\Psi_\lambda}$	Sensitivity factor matrix for power injection, voltage and phase angle
$\mathbf{\Gamma_\omega}$	Covariance matrix of power injection error
Δt	Length of each time slot
$\lambda_{pen,h}$	Penalty price for the heating appliance

Variables

A_{total}	Daily operating cost of the multi-energy system
$b_{n,t}^{ES}$, $b_{i,t}^{GS}$	Binary variables for energy storage systems
$E_{n,t}^{ES}$, $E_{i,t}^{GS}$	The stored energy level of electricity and gas storage
$H_{n,t}^{CHP}$	Heat output of combined heat and power
$H_{h,t}^{D}$	Household heating power
$H_{h,t}^{ext}$	Heating from combined heat and power
$I_{n-m,t}$	Line current magnitude
$L_{i-j,t}^{q}$	Natural gas linepack
$P_{n,t}$, $Q_{n,t}$	Nodal active and reactive power injection
$P_{n,t}^{D}$, $Q_{n,t}^{D}$	Active and reactive power consumption
$P_{n,t}^{G}$, $Q_{n,t}^{G}$	Active and reactive power generation
$P_{n-m,t}$, $Q_{n-m,t}$	Active and reactive power flow
$P_{n,t}^{CHP}$	Power output of combined heat and power
$P_{n,t}^{ES,in}$, $P_{n,t}^{ES,out}$	Electricity storage charge/discharge power
$P_{h,t}^{HP}$, $q_{h,t}^{GF}$	Consumption of heat pump and gas furnace
$P_{n,t}^{RES}$	Active power generation of renewable energy sources
$q_{i,t}$, $p_{i,t}$	Gas nodal injection and pressure
$q_{i,t}^{in}$, $q_{i,t}^{D}$	Gas import flow and consumption
$q_{i-j,t}$, $\psi_{i-j,t}$	Gas flow and direction indicator
$q_{i-j,t}^{CD}$	Gas consumed by compressor
$q_{i,t}^{CHP}$	Gas load of combined heat and power
$q_{i,t}^{GS,in}$, $q_{i,t}^{GS,out}$	Gas storage charge/discharge flow
$T_{h,t}^{in}$, $T_{h,t}^{sf}$	Household interior and surface temperature
$V_{n,t}$, $\theta_{n,t}$	Nodal voltage magnitude and phase angle
$\alpha_{n,k,t}$	Coefficient of corner point combination
$\boldsymbol{\omega}$, $\omega_{n,t}$	Vector and element of power injection error
χ_h , χ	Household penalty and the total penalty associated with heating appliances, respectively

Superscripts

min/max	Minimum or maximum limit of a quantity
$\oplus$, Θ	Forecast expectation and error of a quantity

Weijia Liu and C. Y. Chung are with the Department of Electrical and Computer Engineering, University of Saskatchewan, Saskatoon S7N 5A9, Canada (e-mail: liuweijiamarcel@gmail.com, c.y.chung@usask.ca)

Junpeng Zhan is with the Department of Electrical and Computer Engineering, University of Saskatchewan, Saskatoon S7N 5A9, Canada, and also with the Sustainable Energy Technologies Department, Brookhaven National Laboratory, Upton, NY 11973-5000, USA (email: zhanjunpeng@gmail.com)

Yang Li is with the School of Electrical Engineering, Zhejiang University, Hangzhou 310027, China (email: zjueeliyang@gmail.com)

I. Introduction

In recent years, energy systems structures have appreciably evolved with rapid developments and wide applications of energy conversion technologies to cope with potential energy crises [1]. Especially at the power distribution level, modern power distribution systems (PDSs) are transitioning into sustainable and smart systems with fast-growing numbers of distributed energy resources (DERs) including distributed generations, energy storage systems (ESSs), flexible demands, etc. On the other hand, the volatile and uncertain features of intermittent renewable energy sources (RESs) introduce considerable uncertainties for the secure and economic operation of PDSs [2]. If not handled properly, a PDS may suffer from critical issues including overloading, power shortage, etc. Furthermore, the excessive power generated by RESs may be subject to considerable curtailments due to the absence of coordination among DERs, which also undermines the positive contributions of renewable generation technologies [3].

A promising solution to accommodate the large-scale integration of intermittent RESs is to utilize the flexibility and storage capacities of various DERs in multi-energy carriers to deal with the fluctuations of RES generation [4], [5]. Especially from the energy consumption perspective, multi-energy residential systems (MERSs) are deeply coupled and integrated to accommodate the diverse energy demands of customers. Reasonable operations of MERS will be able to simultaneously improve the utilization efficiency of RES generation capabilities and the reliability of the energy supply to end-users [6], [7].

Considerable research work has been done with respect to the optimal planning and operation of multi-energy systems. For example, the expansion planning of combined electricity and natural gas systems is studied in [8] and [9]; the energy hub concept is proposed in [10] and the optimal energy flow of multiple energy carriers is formulated in [4] and [11]; the operation strategy of a multi-energy system is discussed in [12]-[17]; the residential energy hubs and delivery systems have been studied in [18]-[26]. However, the following research gaps can be identified from existing literature:

- The study on residential energy systems generally emphasizes on either the operation of energy hubs (e.g., in [18], [21], and [26]) or the modelling of energy conversion appliances (e.g., in [19], [21], [22] and [25]). The interactions among different energy distribution systems have not been properly integrated into residential energy system analyses. In addition, the uncertainty factors are mostly handled by time-consuming Monte Carlo simulations that rely heavily on the perfect knowledge of probability distribution functions (PDFs) of random variables in [7], [14], and [22]-[25]. Significant errors will be introduced if the PDFs of uncertain variables are not accurate.
- The models of energy transmission/distribution networks and devices such as gas compressors are nonlinear and nonconvex, which make the MERS models difficult to solve. In existing literature, heuristic optimizations in [8] and [11], decomposed algorithms in [12] and [15], and simplification of gas network and compressor in [9], [13], [23] and [24] are widely used to solve the complex MERS models. However, the computational burden of heuristic and distributed algorithms are quite large, and the existing simplification models may not be applicable for the MERSs.

In this paper, an optimal operation strategy for MERS that considers the interconnected energy networks and the uncertain factors introduced by forecast errors is proposed to bridge these gaps:

- A comprehensive optimization model for a MERS is proposed considering the characteristics of electric power and natural gas distribution networks, RESs, residential appliances, and DERs including ESSs and combined heat and power (CHP) units. A distributionally robust (i.e., robust w.r.t. PDFs) chance-constrained programming (CCP) reformulation method is adopted to model the uncertainties of RES generation, load variation, and energy price fluctuations. Compared to similar uncertainty modelling methods, the distributionally robust reformulation does not assume any specific PDF and only requires the first and second order moments of the uncertain data.
- The nonlinear constraints in the developed MERS model are reformulated and approximated according to the characteristics of a low-voltage PDS and low-pressure natural gas distribution system (NGDS), respectively. Through the proposed reformulation, the CCP-based MERS model becomes a mixed integer second order cone programming (MISOCP) model that is less complex and easier to solve than other models in the existing literature.

The remainder of the paper is organized as follows. Section II discusses the framework and proposes the mathematical model of a MERS. The nonlinear equations and constraints are properly reformulated in Section III. Section IV utilizes a CCP reformulation method to handle the uncertainties associated with RES generation, load consumption, and energy market price. Section V presents numerical simulation results, and the paper is concluded in Section VI.

II. Multi-Energy Residential System Modeling

According to the Canadian household energy usage report, electricity and natural gas together make up around 85% of the total energy consumption [27]. In addition, more than half of the consumed electricity and natural gas is used for heating purposes. Fig. 1 demonstrates a schematic for a typical residential energy system in which energy consumption mainly relies on electricity and natural gas.

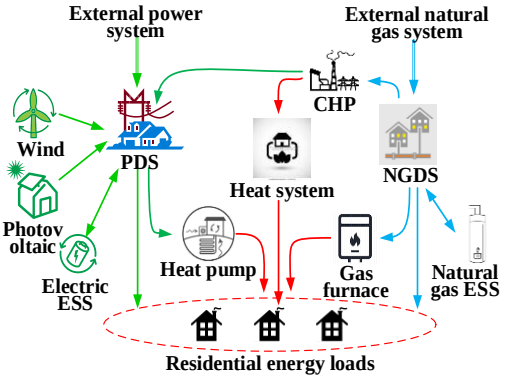

Fig. 1. Schematic of a residential energy system.

A. Day-Ahead Operation Framework

In this paper, the day-ahead operation of the MERS is assumed to be governed by a residential energy system operator (RESO), whose role is similar to the operator of energy hubs as described in [21] and [26]. It is the responsibility of the RESO to participate in day-ahead markets for energy procurement and deliver the desired amount of energy to various consumers in the corresponding residential energy system. In general, the capacity of a residential energy system is much smaller than large generation companies and major industrial customers. Thus, it is reasonable to model the RESO as a price taker in the

day-ahead markets with behaviors that will not influence the market clearing prices.

For a price-taker RESO, the objective in day-ahead operation is to either maximize profit or minimize energy procurement cost based on estimated day-ahead market prices. In this paper, the objective function for a RESO in the day-ahead energy markets is constructed to minimize daily energy procurement costs, which consist of the electricity and natural gas purchasing cost from the external power system and natural gas system. In summary, the objective function of a RESO is described by (1), where a penalty term χ is introduced to punish the RESO if the dispatch of specific loads such as residential heating sources fails to fulfill the satisfaction levels of customers. The penalty term will be discussed in detail in Section II.D.

$$Minimize \quad A_{total} = \sum_{t \in \Omega_T} (\lambda_t^E P_{n_s,t}^G + \lambda_t^G q_{i_s,t}^{in}) \Delta t + \chi \tag{1}$$

B. Modelling of Energy Distribution Systems

1) PDS: The AC power flow is adopted to model the operation of a low-voltage PDS. For simplicity, the well-established AC power flow equations and constraints are generally described by (2) and (3); detailed formulations can be found in Appendix A. The set of variables in PDS operation model is denoted as $\mathbf{X_1}$, where $\mathbf{X_1} = \{ P_{n,t}, Q_{n,t}, V_{n,t}, \theta_{n,t}, I_{n-m,t} \}$.

$$f_{PDS}(P_{n,t}, Q_{n,t}, V_{n,t}, \theta_{n,t}, I_{n-m,t}) = 0 \tag{2}$$

$$g_{PDS}(P_{n,t}, Q_{n,t}, V_{n,t}, \theta_{n,t}, I_{n-m,t}) \le 0 \tag{3}$$

where (2) represents the equations for nodal power injections and branch flows and (3) denotes the constraints of nodal power injection, nodal voltage magnitudes, line current magnitudes, and capacity limit of distribution transformers, respectively.

2) NGDS: The natural gas transmission/distribution system is far more complex than electric power systems. For a low-pressure NGDS, the Pole equation described in [28] is suitable to simulate the steady-state natural gas flow and is adopted in this paper. The Pole equation can be described as:

$$q_{i-j,t} = \varphi_{i-j} \operatorname{sgn}(p_{i,t} - p_{j,t}) \sqrt{| p_{i,t} - p_{j,t} |} \tag{4}$$

Similarly, the steady-state operation of the NGDS can be generally described by (5) and (6), detailed formulations can be found in [28] and will not be further discussed.

$$f_{NGDS}(q_{i,t}, p_{i,t}, q_{i-j,t}) = 0 \tag{5}$$

$$g_{NGDS}(q_{i,t}, p_{i,t}, q_{i-j,t}) \le 0 \tag{6}$$

where (5) represents the nodal natural gas injection equation, (6) denotes the constraints of the source node inlet flow rate, nodal gas pressures, and pipeline gas flow rate, respectively.

Unlike an electric power system, the natural gas production does not have to be identical to consumption in the real time. The natural gas pipelines will automatically function as gas storage units, which is generally denoted as linepack [16], [29]. The linepack is calculated by (7) and constrained by (8):

$$L_{i-j,t}^q = \frac{2}{3} \mu_{i-j} \frac{p_{i,t}^3 - p_{j,t}^3}{p_{i,t}^2 - p_{j,t}^2} = \frac{2}{3} \mu_{i-j} (p_{i,t} + p_{j,t} - \frac{p_{i,t} p_{j,t}}{p_{i,t} + p_{j,t}}) \tag{7}$$

$$L_{i-j,t}^{q,\min} \le L_{i-j,t}^q \le L_{i-j,t}^{q,\max} \tag{8}$$

where the lower and upper linepack limits in (8) can be respectively calculated by (9) and (10) based on the Pole equation (4) and the definition given in [16]:

$$L_{i-j,t}^{q,\min} = \frac{2}{3} \mu_{i-j} \frac{(p_j^{\min} + \varphi_{i-j}^{-2} (q_{i-j,t})^2)^3 - (p_j^{\min})^3}{(p_j^{\min} + \varphi_{i-j}^{-2} (q_{i-j,t})^2)^2 - (p_j^{\min})^2} \tag{9}$$

$$L_{i-j,t}^{q,\max} = \frac{2}{3} \mu_{i-j} \frac{(p_i^{\max})^3 - (p_i^{\max} - \varphi_{i-j}^{-2} (q_{i-j,t})^2)^3}{(p_i^{\max})^2 - (p_i^{\max} - \varphi_{i-j}^{-2} (q_{i-j,t})^2)^2} \tag{10}$$

In addition, compressors are also key equipment in the natural gas system. In this paper, it is assumed that the power demand of a compressor is supplied by its associated gas motor, and is independent of the PDS. The consumption of a compressor can be calculated by (11), and (12) constrains that the outlet pressure of compressor is not smaller than the inlet pressure.

$$q_{i-j,t}^{CD} = \frac{\tau q_{i-j,t} \beta}{\eta(\beta - 1)} \left[\left(\frac{p_{j,t}}{p_{i,t}} \right)^{(\beta-1)/\beta} - 1 \right] \tag{11}$$

$$p_{j,t} \ge p_{i,t} \tag{12}$$

The set of variables in the NGDS operation model is denoted as $\mathbf{X_2}$, where $\mathbf{X_2} = \{ q_{i,t}, q_{i-j,t}, p_{i,t}, L_{i-j,t}^q, q_{i-j,t}^{CD} \}$.

C. Modelling of DERs

1) CHP Units: The electric power generation and heat production of a CHP unit are deeply coupled. From the day-ahead operation point of view, the most important issue to be addressed when modelling the output characteristics of a CHP unit is to develop the connection between the electric power and heat production. In this paper, a commonly used feasible operation region, which is usually represented by a polytope, is utilized to link the electric power and heat production of a gas-turbine based CHP unit in a two-dimensional space [30].

The feasible operation region of a CHP unit is generally constrained by the maximum/minimum inlet gas flow, maximum heat production, etc. In the existing literature, the feasible operation region can be modeled by a convex or non-convex irregular quadrilateral with one or several segments. As indicated in [31], a convex, single-segment, irregular quadrilateral shape is most appropriate for modeling gas-turbine-based CHP units. As a result, the single-segment irregular quadrilateral feasible region can be described through a convex combination of all corner points of the quadrilateral [32]. The four corner points of the quadrilateral are, respectively, the: 1) the maximum electric power output at the minimum gas inlet; 2) the maximum electric power output at the maximum gas inlet; 3) the maximum heat production at the minimum gas inlet; and 4) the maximum heat production at the maximum gas inlet.

In summary, the feasible operation region of a CHP unit can be expressed as:

$$P_{n,t}^{CHP} = \sum_{k \in \Omega_K} \alpha_{n,k,t} P_{n,k}^{CHP} \tag{13}$$

$$H_{n,t}^{CHP} = \sum_{k \in \Omega_K} \alpha_{n,k,t} H_{n,k}^{CHP} \tag{14}$$

$$q_{i,t}^{CHP} = \sum_{n \to i} \sum_{k \in \Omega_K} \alpha_{n,k,t} q_{n,k}^{CHP} \tag{15}$$

$$0 \le \alpha_{n,k,t} \le 1 \tag{16}$$

$$\sum_{k \in \Omega_K} \alpha_{n,k,t} = 1 \tag{17}$$

where $n \to i$ represents all of the residential districts that belong to PDS node *n* and NGDS node *i*. $P_{n,k}^{CHP}$, $H_{n,k}^{CHP}$, and $q_{n,k}^{CHP}$ denote the electric power generation, heat production, and gas consumption of the *k*-th corner point, respectively. Equations (13)-(15) calculate the power output, heat output, and natural gas load of CHP, respectively. Equations (16) and (17) ensure that the operating point of CHP always falls into the CHP's feasible operation region.

The set of variables in the CHP operation model is denoted

as $\mathbf{X_3}$, where $\mathbf{X_3}=\{P_{n,t}^{CHP}, H_{n,t}^{CHP}, q_{i,t}^{CHP}, \alpha_{n,k,t}\}$. The heat production of CHP units is assumed to be utilized by their adjacent residential nodes as district heating sources, which will be further discussed in later sections.

2) Residential Heating Sources: The heating demand is generally regarded as a significant component of total residential energy consumption. So far, heat pumps (HPs) that consume electricity and gas furnaces (GFs) that consume natural gas are the two most popular residential heating sources. The heat production of an HP or a GF can be described by:

$$H_{h,t}^{D}=\gamma_h^{HP}\eta_h^{HP}P_{h,t}^{HP}+\gamma_h^{GF}\eta_h^{GF}q_{h,t}^{GF} \tag{18}$$

By operating the heating appliances, the interior temperatures of residential houses should be kept within certain intervals to accommodate the comfort requirements of customers. A linearized thermal house model is introduced to simulate the indoor temperature profiles [33]:

$$\begin{aligned}(T_{h,t}^{in}-T_{h,t-\Delta t}^{in})\Delta t^{-1}=(C_h^{in})^{-1}[&H_{h,t}^{D}+H_{h,t}^{ext}+H_{h,t}^{in,rad}\\&+\zeta_h^{is}(T_{h,t}^{sf}-T_{h,t}^{in})+\zeta_h^{ie}(T_t^{ext}-T_{h,t}^{in})]\end{aligned} \tag{19}$$

$$\begin{aligned}(T_{h,t}^{sf}-T_{h,t-\Delta t}^{sf})\Delta t^{-1}=(C_h^{sf})^{-1}[&\zeta_h^{se}(T_t^{ext}-T_{h,t}^{sf})\\&+H_{h,t}^{sf,rad}+\zeta_h^{is}(T_{h,t}^{in}-T_{h,t}^{sf})]\end{aligned} \tag{20}$$

$$\sum_{h\in\Omega_{CHP}^{n}}H_{h,t}^{ext}=H_{n,t}^{CHP} \tag{21}$$

where (19) and (20) evaluate the household indoor and surface temperatures, respectively. Equation (21) constrains that the external household heating is obtained from the heat production of CHP.

The indoor temperature, household heating power, and heating from CHP should accommodate the following constraints:

$$T_h^{in,\min}\le T_{h,t}^{in}\le T_h^{in,\max} \tag{22}$$

$$0\le H_{h,t}^{D}\le H_h^{D,\max} \tag{23}$$

$$0\le H_{h,t}^{ext}\le H_h^{ext,\max} \tag{24}$$

As another heating option for residential houses, the dual fuel heating solution normally combines an HP and a GF as heating sources. Typically, HPs are more efficient than GFs when the ambient temperature is above the balance temperature (normally ranges from 30°F to 40°F). If the ambient temperature drops below this level, GFs will be automatically switched on to replace HPs. In summary, the operation of dual fuel heating appliances can be expressed as:

$$\begin{cases}if\ T_t^{ext}\ge T_{balance}^{ext} & \gamma_h^{HP}=1,\ \gamma_h^{GF}=0\\ Otherwise & \gamma_h^{HP}=0,\ \gamma_h^{GF}=1\end{cases} \tag{25}$$

The set of variables of the heating appliance model is denoted as $\mathbf{X_4}$, where $\mathbf{X_4}=\{P_{h,t}^{HP}, q_{h,t}^{GF}, H_{h,t}^{D}, H_{h,t}^{ext}, T_{h,t}^{in}, T_{h,t}^{sf}\}$.

3) ESSs: Storage systems for both electric power and natural gas can be modeled according to their storage capacity, charging/discharging flow limitations, and efficient factors. Thus, the operation of ESSs can be described as:

$$E_{n,t}^{ES}-E_{n,t-\Delta t}^{ES}=(\eta^{ES,in}P_{n,t}^{ES,in}-(\eta^{ES,out})^{-1}P_{n,t}^{ES,out})\Delta t \tag{26}$$

$$E_{n,t}^{GS}-E_{n,t-\Delta t}^{GS}=(\eta^{GS,in}q_{i,t}^{GS,in}-(\eta^{GS,out})^{-1}q_{i,t}^{GS,out})\Delta t \tag{27}$$

$$E_n^{ES,\min}\le E_{n,t}^{ES}\le E_n^{ES,\max},\quad E_i^{GS,\min}\le E_{i,t}^{GS}\le E_i^{GS,\max} \tag{28}$$

$$0\le P_{n,t}^{ES,in}\le b_{n,t}^{ES}P_n^{ES,in,\max},\ 0\le P_{n,t}^{ES,out}\le(1-b_{n,t}^{ES})P_n^{ES,out,\max} \tag{29}$$

$$0\le q_{i,t}^{GS,in}\le b_{i,t}^{GS}q_i^{GS,in,\max},\ 0\le q_{i,t}^{GS,out}\le(1-b_{i,t}^{GS})q_i^{GS,out,\max} \tag{30}$$

$$E_{n,t_{end}}^{ES}-E_{n,t_{start}}^{ES}\ge 0,\ E_{i,t_{end}}^{GS}-E_{i,t_{start}}^{GS}\ge 0 \tag{31}$$

$$b_{n,t}^{ES},\ b_{i,t}^{GS}\in\{0,1\} \tag{32}$$

where the quantities of stored energy in ESSs are calculated by (26) and (27) and constrained by (28). Equations (29) and (30) constrain the charging/discharging energy flow of ESSs based on two introduced binary variables to avoid unrealistic simultaneous charging and discharging behaviors. Equation (31) guarantees the consistency of ESS operations.

The set of binary and continuous variables of ESS models are respectively denoted as $\mathbf{Y_1}$ and $\mathbf{X_5}$, where $\mathbf{Y_1}=\{b_{n,t}^{ES}, b_{i,t}^{GS}\}$ and $\mathbf{X_5}=\{E_{n,t}^{ES}, P_{n,t}^{ES,in}, P_{n,t}^{ES,out}, E_{n,t}^{GS}, q_{i,t}^{GS,in}, q_{i,t}^{GS,out}\}$, respectively.

D. Flexible Demand Related Penalty

The residential heating sources discussed in Section II.C are regarded as flexible loads, as their energy consumptions can be adjusted as long as their key parameters accommodate their corresponding limits (i.e., $T_{h,t}^{in}$ accommodates constraint (22)). However, the cost minimization (profit maximization) objective is likely to lead to heating appliances minimizing (maximizing) their consumptions and $T_{h,t}^{in}$ constrained at its lower limit $T_h^{in,\min}$ (higher limit $T_h^{in,\max}$) most of the time, which will affect the satisfaction levels of customers. In these cases, the RESO should provide additional compensation to these customers despite the fact that constraint (22) is accommodated.

To deal with this issue, a penalty term χ is added to the objective function as described in (1). The penalty for household *h* is defined as χ_h in (33), and χ_h becomes greater than zero if the daily average $T_{h,t}^{in}$ is lower than a threshold value that represents the satisfaction level. In this paper, the mean value of the feasible interval $[T_h^{in,\min}, T_h^{in,\max}]$ is selected as the threshold for χ_h. The penalty function is formulated in (34) to charge the RESO if the satisfaction levels of customers are affected (χ_h is greater than zero). The set of variables is denoted as $\mathbf{X_6}$ where $\mathbf{X_6}=\{\chi_h, \chi\}$.

$$\chi_h\ge\sum_{t\in\Omega_T}\left(\frac{T_{h,t}^{in,\max}+T_{h,t}^{in,\min}}{2}-T_{h,t}^{in}\right),\quad \chi_h\ge 0 \tag{33}$$

$$\chi=\sum_{h\in\Omega_H}\lambda_{pen,h}\chi_h \tag{34}$$

In summary, the developed MERS model is a mixed integer nonlinear programming (MINLP) model, which is described as follows:

$$\min_{\mathbf{X_1},\mathbf{X_2},\mathbf{X_3},\mathbf{X_4},\mathbf{X_5},\mathbf{X_6},\mathbf{Y_1}}\ (1)$$

$$s.t.\ (2)\text{-}(34)$$

$$\mathbf{X_1},\mathbf{X_2},\mathbf{X_3},\mathbf{X_4},\mathbf{X_5},\mathbf{X_6}\in\mathbb{R},\ \mathbf{Y_1}\in\mathbb{Z}$$

III. Reformulation of Energy System Models

The MERS model proposed in Section II is an MINLP model, which is difficult to solve in a timely manner. Piecewise linearization is widely utilized in existing research to linearize and approximate the nonlinear constraints of natural gas systems (e.g., in [23] and [24]) and power systems (e.g., in [34]). However, the implementation of the piecewise linearization method will introduce a significant number of binary variables. Since low-voltage PDSs and low-pressure NGDSs are considered in the residential energy systems, this section employs linearization and relaxation methods based on features of PDS and NGDS to reformulate the MERS model and reduce the computation burden.

A. PDS and NGDS Models

The PDS normally operates as a radial network, thus the conventional AC power flow equations in (2) and (3) can be effectively relaxed as a second order cone programming (SOCP) problem [35], [36]. The SOCP relaxation is described in Appendix B. After relaxation, the original $\mathbf{X_1}$ is replaced with $\mathbf{X_1^*}$, the details of which are also provided in Appendix B.

The Pole equation in (4) contains sign function and root square, and can be relaxed by introducing binary variables as:

$$q_{i-j,t}^2 \le \varphi_{i-j}^2 (p_{i,t} - p_{j,t}) + M(1-\psi_{i-j,t}) \tag{35}$$

$$q_{i-j,t}^2 \le M\psi_{i-j,t} \tag{36}$$

$$p_{i,t} - p_{j,t} \le M\psi_{i-j,t} \tag{37}$$

$$\psi_{i-j,t} + \psi_{j-i,t} = 1 \tag{38}$$

$$\psi_{i-j,t} \in \{0,1\} \tag{39}$$

where (35) and (36) relax the Pole equation (4), and (37)-(39) utilize binary variables to indicate gas flow directions. Note that the proposed (35)-(39) is also an SOCP relaxation. Compared to the NGDS model (4)-(6), the set of newly introduced binary variables is denoted as $\mathbf{Y_2}$ where $\mathbf{Y_2} = \{\psi_{i-j,t}\}$.

B. Linepack and Compressor Models

For the low-pressure NGDSs where the differences among nodal pressures are limited, it is reasonable to assume that nodal gas pressures do not vary significantly from their reference points. These reference points can be derived from historical average values (if historical data is available), or from their highest/lowest limits according to the operating pressure at the NGDS source node. Thus, a linear approximation method is adopted to approximate the linepack and compressor based on Taylor series. Assume a nonlinear function $g(x,y)$ is derivable at a reference point $(\bar{x}, \bar{y})$, $g(x,y)$ can be approximated as:

$$g(x,y) \approx g(\bar{x},\bar{y}) + \partial g_x(\bar{x},\bar{y})(x-\bar{x}) + \partial g_y(\bar{x},\bar{y})(y-\bar{y}) \tag{40}$$

Based on (40), the linepack volume equation (7) can be approximated by (41). The linepack limits (9) and (10) can be similarly approximated as demonstrated in (42) and (43), respectively. Although $L_{i-j,t}^{q,\max}$ and $L_{i-j,t}^{q,\min}$ are still nonlinear after employing (40), the linepack constraint (8) becomes a convex conic constraint that marginally contributes to the computational burden.

$$L_{i-j,t}^{q} \approx \frac{2\mu_{i-j}}{3}(p_{i,t} + p_{j,t} - \frac{p_{i,t}+p_{j,t}}{4}) = \frac{\mu_{i-j}(p_{i,t}+p_{j,t})}{2} \tag{41}$$

$$L_{i-j,t}^{q,\max} \approx \mu_{i-j} p_i^{\max} - 0.5\varphi_{i-j}^{-2} q_{i-j,t}^2 \tag{42}$$

$$L_{i-j,t}^{q,\min} \approx \mu_{i-j} p_j^{\min} + 0.5\varphi_{i-j}^{-2} q_{i-j,t}^2 \tag{43}$$

On the other hand, by using the approximation (40), the consumption of compressor in (11) can be approximated as (44) with two bilinear components.

$$\begin{aligned} q_{i-j,t}^{CD} &\approx \frac{\tau q_{i-j,t}\beta}{\eta(\beta-1)}\left[\left(1+\frac{(\beta-1)(p_{j,t}-p_{i,t})}{\beta p_i^{\max}}\right)-1\right] \\ &= \frac{q_{i-j,t}(p_{j,t}-p_{i,t})}{\tau^{-1}\eta p_i^{\max}} = \frac{p_j^{\max} q_{i-j,t} - q_{i-j,t} p_{i,t}}{\tau^{-1}\eta p_i^{\max}} \end{aligned} \tag{44}$$

For simplicity, it is assumed that the outlet pressure of a compressor always equals to the maximum nodal gas pressure, then (44) only contains one bilinear component $q_{i-j,t}p_{i,t}$. The bilinear components can be convexly relaxed by the widely used McCormick envelopes. However, the gas flow through a compressor has a wide feasible range, thus the McCormick method may introduce significant errors. Piecewise linearization methods are commonly employed in existing literature to improve the accuracy of McCormick envelopes. However, a large number of binary variables are involved in piecewise linearization methods when solving a large-scale optimization problem, which significantly affects the computational efficiency. Alternatively, the bilinear part $q_{i-j,t}p_{i,t}$ can be approximated by (40) as well. Since the compressor outlet pressure is fixed at maximum nodal pressure, the compressor gas flow is generally negatively correlated with the compressor inlet pressure. Thus the reference point of the considered compressor will be selected at maximum flow and minimum inlet pressure. Note that the inlet pressure at maximum gas flow may not necessarily equal to $p_i^{\min}$. To enhance the accuracy of linear approximation, one run of natural gas flow with maximum compressor flow will be processed prior to solving the proposed model to obtain the minimum compressor inlet pressure, denoted as $p_{i,t}^{*\min}$. Then $q_{i-j,t}p_{i,t}$ can be approximated at the reference point $(q_{i-j}^{\max}, p_{i,t}^{*\min})$, shown as:

$$q_{i-j,t}p_{i,t} \approx q_{i-j}^{\max} p_{i,t} + p_{i,t}^{*\min} q_{i-j,t} - q_{i-j}^{\max} p_{i,t}^{*\min} \tag{45}$$

Thus, the compressor consumption in (11) is linearized as:

$$\begin{aligned} q_{i-j,t}^{CD} &\approx \frac{p_j^{\max} q_{i-j,t} - q_{i-j,t} p_{i,t}}{\tau^{-1}\eta p_i^{\max}} \\ &\approx \frac{(p_j^{\max} - p_{i,t}^{*\min}) q_{i-j,t} - q_{i-j}^{\max} p_{i,t} + q_{i-j}^{\max} p_{i,t}^{*\min}}{\tau^{-1}\eta p_i^{\max}} \end{aligned} \tag{46}$$

C. ESSs Models

In Section II.C, binary variables are introduced to constrain operating statuses of ESSs. To reduce the total number of binary variables used in the reformulated MERS model, a relaxation method is proposed in this section. Take electricity storage as an example, the constraints (26) and (29) can be relaxed as:

$$E_{n,t}^{ES} - E_{n,t-\Delta t}^{ES} \le \eta^{ES,in}(P_{n,t}^{ES,in} - P_{n,t}^{ES,out})\Delta t \tag{47}$$

$$E_{n,t}^{ES} - E_{n,t-\Delta t}^{ES} \le (\eta^{ES,out})^{-1}(P_{n,t}^{ES,in} - P_{n,t}^{ES,out})\Delta t \tag{48}$$

$$0 \le P_{n,t}^{ES,in} \le P_n^{ES,in,\max},\ 0 \le P_{n,t}^{ES,out} \le P_n^{ES,out,\max} \tag{49}$$

Since the ESS charging efficiency $\eta^{ES,in}$ and discharging efficiency $\eta^{ES,out}$ are both smaller than 1, (48) or (47) will be relaxed when the storage is charging or discharging, respectively. As a result, (26) and (29) can be relaxed and $b_{n,t}^{ES}$ can be omitted. Equations (27) and (30) can be handled similarly to eliminate $b_{i,t}^{GS}$ as described by (50)-(52).

$$E_{i,t}^{GS} - E_{i,t-\Delta t}^{GS} \le \eta^{GS,in}(q_{i,t}^{GS,in} - q_{i,t}^{GS,out})\Delta t \tag{50}$$

$$E_{i,t}^{GS} - E_{i,t-\Delta t}^{GS} \le (\eta^{GS,out})^{-1}(q_{i,t}^{GS,in} - q_{i,t}^{GS,out})\Delta t \tag{51}$$

$$0 \le q_{i,t}^{GS,in} \le q_i^{GS,in,\max},\ 0 \le q_{i,t}^{GS,out} \le q_i^{GS,out,\max} \tag{52}$$

IV. Reformulation of Chance Constraints

The optimal operation of energy systems depends greatly on the forecast of RES generation, load consumption, and energy price. The CCP and its linear reformulation method proposed in [37] will be employed to model the uncertainties introduced by the forecast errors.

A. Uncertainty of Generation and Consumption

Uncertainties of RES generation and load forecast will directly influence the nodal active power injection and further

affect the AC power flow constraint (3) in the PDS concerned. For each variable in constraint (3) (excluding $\theta_{n,t}$ since $I_{n-m,t}$ is normally used in PDSs), the formulation of chance constraints can be written as:

$$\mathbb{P}\{P_{n,t}^{\min} \le P_{n,t} \le P_{n,t}^{\max}\} \ge 1-\phi_P \tag{53}$$

$$\mathbb{P}\{Q_{n,t}^{\min} \le Q_{n,t} \le Q_{n,t}^{\max}\} \ge 1-\phi_Q \tag{54}$$

$$\mathbb{P}\{(V_n^{\min})^2 \le (V_{n,t})^2 \le (V_n^{\max})^2\} \ge 1-\phi_V \tag{55}$$

$$\mathbb{P}\{(I_{n-m,t})^2 \le (I_{n-m}^{\max})^2\} \ge 1-\phi_I \tag{56}$$

where constraints (55) and (56) have already been modified to accommodate the SOCP relaxation as described in Appendix B.

Among all the variables in (53)-(56), $P_{n,t}$ can be directly expressed by the forecast values and errors as shown in (57), and (53) can be rewritten as (58).

$$P_{n,t} = P_{n,t}^{\oplus} + P_{n,t}^{\Theta RES} - P_{n,t}^{\Theta D,fix} = P_{n,t}^{\oplus} + \omega_{n,t} \tag{57}$$

$$\mathbb{P}\{\mathbf{P^{min}} \le \mathbf{P}^{\oplus} + \mathbf{\Psi_P \omega} \le \mathbf{P^{max}}\} \ge 1-\phi_P \tag{58}$$

In (58), $\mathbf{\Psi_P}$ reflects the sensitivity of nodal active power injection to the variations of $\boldsymbol{\omega}$. $\mathbf{\Psi_Q}$ can be similarly obtained [38,39]. $\mathbf{\Psi_V}$ and $\mathbf{\Psi_I}$ can be derived from AC power flow Jacobians, which depend on the nominal operating statuses of the PDS. Thus, $\mathbf{\Psi_V}$ and $\mathbf{\Psi_I}$ should be approximated before optimizing the reformulated CCP model.

Since the deviations of active/reactive power injection, voltage, and current magnitudes have been represented by coefficient matrixes and forecast error $\boldsymbol{\omega}$, the chance constraints (53)-(56) can be linearized. Take (53) as an example, (53) can be reformulated as:

$$\mathbf{P}^{\oplus} \le \mathbf{P^{max}} - f^{-1}(1-\phi_P)\sqrt{\mathbf{\Psi_P \Gamma_\omega \Psi_P^T}} \tag{59}$$

$$\mathbf{P}^{\oplus} \ge \mathbf{P^{min}} + f^{-1}(1-\phi_P)\sqrt{\mathbf{\Psi_P \Gamma_\omega \Psi_P^T}} \tag{60}$$

where f^{-1} is the inverse cumulative distribution function (ICDF). Similarly, (54)-(56) are linearized as follows:

$$\mathbf{Q} \le \mathbf{Q^{max}} - f^{-1}(1-\phi_Q)\sqrt{\mathbf{\Psi_Q \Gamma_\omega \Psi_Q^T}} \tag{61}$$

$$\mathbf{Q} \ge \mathbf{Q^{min}} + f^{-1}(1-\phi_Q)\sqrt{\mathbf{\Psi_Q \Gamma_\omega \Psi_Q^T}} \tag{62}$$

$$\mathbf{V}^2 \le (\mathbf{V^{max}} - f^{-1}(1-\phi_V)\sqrt{\mathbf{\Psi_V \Gamma_\omega \Psi_V^T}})^2 \tag{63}$$

$$\mathbf{V}^2 \ge (\mathbf{V^{min}} + f^{-1}(1-\phi_V)\sqrt{\mathbf{\Psi_V \Gamma_\omega \Psi_V^T}})^2 \tag{64}$$

$$\mathbf{I}^2 \le (\mathbf{I^{max}} - f^{-1}(1-\phi_I)\sqrt{\mathbf{\Psi_I \Gamma_\omega \Psi_I^T}})^2 \tag{65}$$

B. Uncertainty of Energy Price

The energy price of natural gas generally establishes on long-term fixed-price contracts, while the energy price of electric power may vary significantly throughout one operating day. To accommodate the uncertainty of electricity price, system operator still minimizes A_{total} as demonstrated in (1), while the following constraints will be added:

$$\mathbb{P}\{A_{total} \ge A_{total}^{\oplus} + \sum_{t\in\Omega_T} \lambda_t^{\Theta E} P_{n_s,t}^{G} \Delta t\} \ge 1-\phi_\lambda \tag{66}$$

$$A_{total}^{\oplus} = \sum_{t\in\Omega_T} (\lambda_t^{\oplus E} P_{n_s,t}^{G} + \lambda_t^{G} q_{i_s,t}^{in})\Delta t + \chi \tag{67}$$

Employing the aforementioned CCP reformulation method and assuming the energy price forecast errors at different time slots are not correlated, (66) can be rewritten as (68), where $\| \|_2$ denotes the Euclidean norm.

$$A_{total} \ge A_{total}^{\oplus} + f^{-1}(1-\phi_\lambda)\left\|\mathbf{\Psi_\lambda}\right\|_2 \tag{68}$$

Note that $\mathbf{\Psi_\lambda}$ is dependent on the $P_{n_s,t}^{G}$, and should also be approximated before optimizing the reformulated CCP model.

C. Solving the Reformulated CCP

Using the proposed linearization and approximation methods in Sections III and IV, the reformulated CCP-based MERS model becomes an MISOCP model and is further denoted as the *reformulated model* in this paper. The reformulated model is described as follows:

$$\min_{\mathbf{X_1^*, X_2, X_3, X_4, X_5, X_6, Y_2}} \quad (1)$$

$$s.t. \quad (6),(8),(12),(13)\text{-}(25),(28),(31),(33),$$
$$(34)\text{-}(39),(41)\text{-}(43),(46)\text{-}(52),(59)\text{-}(65),$$
$$(67),(68),(A1),(A2),(A9)\text{-}(A14),(A17)$$
$$\mathbf{X_1^*, X_2, X_3, X_4, X_5, X_6} \in \mathbb{R},\ \mathbf{Y_2} \in \mathbb{Z}$$

where constraints (A1), (A2), (A9)-(A14), and (A17) are relaxed power flow constraints, the details of which can be found in Appendices A and B.

Traditional uncertainty modelling methods, such as CCP, highly depend on the knowledge of PDFs. In this day-ahead operation of the MERS case, the calculation of ICDF depends on the PDFs of RES generation and load forecast errors, which is straightforward if the PDFs are already known to the operator. However, these PDFs can only be approximated with satisfactory accuracy when there are sufficient data. In fact, the RESs have been recently introduced to residential energy systems and their data are very limited in general. Thus, the approximated PDFs are inaccurate and will bring additional risks to the RESO. In this regard, a distributionally robust estimation based on Chebyshev's inequality will be employed [40], which only relies on knowledge of the first and second order moments of the random data. For any given confidence level ϕ, ICDF can be calculated with:

$$f^{-1}(1-\phi) = \sqrt{\phi^{-1}(1-\phi)} \tag{69}$$

Combining (59)-(65) and (68) with (69), the reformulated CCP is robust to the PDFs of uncertain data. This is especially beneficial to RESOs with insufficient data for RES generation. The advantages of distributionally robust CCP reformulation will be further investigated in the case studies.

To approximate $\mathbf{\Psi_V}$, $\mathbf{\Psi_I}$, and $\mathbf{\Psi_\lambda}$, the AC power flow will be calculated first based on forecasted data at each time interval to obtain system Jacobians and $P_{n_s,t}^{G}$. Solving the proposed reformulated model consists of the following steps:

1) Forecast $P_{n,t}^{\oplus RES}$ and $P_{n,t}^{\oplus D,fix}$ for the next operating day.
2) Solve AC power flow based on $P_{n,t}^{\oplus RES}$ and $P_{n,t}^{\oplus D,fix}$.
3) Obtain approximated $\mathbf{\Psi_V}$, $\mathbf{\Psi_I}$, and $\mathbf{\Psi_\lambda}$.
4) Solve the proposed reformulated model.

V. Case Study

A. Case Study Setup

The test energy system illustrated in Fig. 2 consists of an IEEE 33-bus PDS and a 14-bus NGDS. The parameters of DERs in both systems are listed in Table I. The rating voltage of the 33-bus PDS is 10 kV, with a distribution transformer capacity of 5 MVA at node 1, and each node has 4 residential houses. The natural gas supply rate from the NGDS source node is fixed at 80 m^3/h, and a compressor connects node 1 and node 13 to formulate a unidirectional gas flow from node 1 to node

13. Two CHP units located at nodes 3 and 11 in the PDS consume natural gas from nodes 2 and 9 from the NGDS, respectively. Table II also lists some important input parameters, while the data for the NGDS, household heating sources, and RES generation outputs are derived from [28], [33], and [41], respectively. The penalty price $\lambda_{pen,h}$ and confidence level ϕ are set to 0.05 \$/*h* °C and 0.05, respectively. Δt is set to 15 minutes.

Assuming the forecast errors of RES generation, loads and energy prices are symmetric with zeros means and standard deviation equaling 5%, 2%, and 2% of the corresponding forecasted values, respectively. When calculating $\mathbf{\Gamma}_{\omega}$, the generation of the two PVUs are assumed to be fully correlated, while the correlation coefficient between the wind power unit (WPU) and photovoltaic units (PVUs) are –0.25. The load variations at different nodes are assumed to be independent of each other.

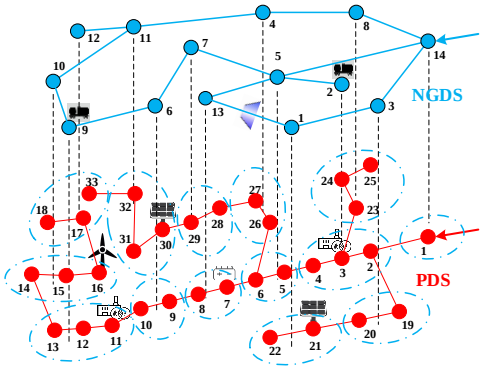

Fig. 2. Test system topologies: 33-bus PDS and 14-bus NGDS

TABLE I
PARAMETERS OF DERS IN RESIDENTIAL ENERGY SYSTEM

Name	Node	Capacity	Rating power
WPU	PDS-16	1000 kVA	800 kW
PVU 1	PDS-21	800 kVA	600 kW
PVU 2	PDS-30	800 kVA	600 kW
Electricity storage	PDS-7	150 kWh	300 kW
Gas storage 1	NGDS-3	30 m^3	10 m^3/h
Gas storage 2	NGDS-11	30 m^3	10 m^3/h

TABLE II
SIMULATION PARAMETERS

$T_h^{in,\max}$, $T_h^{in,\min}$ (°C)	24, 20	$H^{D,\max}$ (kW)	15.15
$E^{ES,\max}$, $E^{GS,\max}$ (%)	90	$H^{ext,\max}$ (kW)	10
$E^{ES,\min}$, $E^{GS,\min}$ (%)	10	η_h^{HP}, η_h^{GF} (%)	400, 80
$V_n^{\max}$, $V_n^{\min}$ (p.u.)	1.1, 0.9	$\eta^{ES,in}$, $\eta^{ES,out}$, $\eta^{GS,in}$, $\eta^{GS,out}$ (%)	95

B. Simulation Results

The proposed reformulated model is solved by GAMS/CPLEX on a desktop computer with a quad-core 3.6GHz processor and 12GB memory. It takes around 2s to preprocess the AC Jacobians of all operating intervals, and the average solving time of the reformulated model is 76.4s.

For comparison, the case study setup in Section V.A is referred to as the *base case setup*, and the optimal solution to the reformulated model in the base case setup is referred to as *case 0*. Table III lists the simulation statistics of case 0.

The total daily energy costs at various confidence levels are compared in Fig. 3. When the confidence level $(1-\phi)$ increases, the generation of RES will be dispatched more conservatively and the RESO will be forced to purchase more energy from the market. Thus, the daily energy cost increases with the increase of confidence level, as illustrated in Fig. 3.

TABLE III
STATISTICS OF OPTIMIZED STRATEGY OF CASE 0

Daily energy cost (\$)					
Total	2794.36	PDS	2347.05	χ	5.23
Daily active power injection (MWh)					
External	13.86	RES	8.81	CHP	0.67
Daily heat production (MWh)					
CHP	0.19	HP	7.67	GF	8.11
Daily power loss (kWh)					
PDS	437.62	ESS	7.68		
Daily natural gas loss (m^3)					
Compressor	1.43	ESS	2.41		

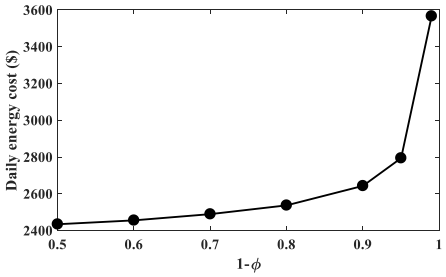

Fig. 3. Daily energy cost profiles at various confidence levels.

On the other hand, $\lambda_{pen,h}$ has a substantial impact on the schedules of household heating appliances and the average indoor temperature profile. Table IV compares some key parameters with different $\lambda_{pen,h}$ values, while other parameters are the same as the base case setup. Table IV shows the average indoor temperature is significantly lower than the selected comfort threshold (22°C) when $\lambda_{pen,h}$ equals zero. Although constraint (22) is accommodated, this optimized operation strategy is not desirable, especially for customers. With increasing $\lambda_{pen,h}$, the average indoor temperature rises and so does the total daily energy cost. When $\lambda_{pen,h}$ equals 0.5 \$/*h* °C or becomes even larger, the deficit between the average indoor temperature and the comfort threshold becomes negligible.

The effectiveness of the reformulated model and the impact of various DERs are further verified by modifying the base case setup. The following cases are simulated and compared in Table V:

- Case 1: Base case setup with a more volatile electricity market price. The average daily price and standard deviation of price in case 0 (case 1) are 0.17 \$/kWh (0.17 \$/kWh) and 0.05 \$/kWh (0.22 \$/kWh), respectively.
- Case 2: Base case setup with exterior temperature increased by 5°C at each time slot.
- Case 3: Base case setup with exterior temperature decreased by 5°C at each time slot.

Table V shows the total energy cost of case 1, where the electricity price suffers from more severe fluctuations is much lower than that for case 0. Because the average daily electricity prices of these two cases are the same, the higher deviation of price data in case 1 indicates more significant deficits between price peaks and valleys. The optimized schedule increases its energy procurement at price valley hours and decreases its consumption at price peak hours. By doing so, the reliance on CHPs and ESSs is relieved, and the total energy bill is significantly reduced although the total electricity procurement is increased as demonstrated in Table V.

TABLE IV
OPTIMIZED OPERATION STRATEGIES WITH VARIOUS $\lambda_{pen,h}$

$\lambda_{pen,h}$ ($/h °C)	χ ($)	Average indoor temperature (°C)	Total daily energy cost ($)
0	0	20.97	2737.40
0.01	22.64	21.28	2767.19
0.02	28.40	21.55	2785.60
0.05	5.23	21.97	2794.36
0.1	1.86	21.99	2796.37
0.5	0.55	22.00	2799.86
1.0	0.26	22.00	2801.97

TABLE V
COMPARISON OF OPTIMIZED OPERATION STRATEGIES OF CASES 0, 1, 2, AND 3

Case	Daily energy cost ($)	RES generation (MWh)	External electricity procurement (MWh)	CHP power generation (MWh)	CHP heat production (MWh)
0	2794.36	8.81	13.86	0.67	0.19
1	2352.20	8.78	14.41	0.63	0.12
2	2690.87	8.78	13.19	0.88	0.26
3	2955.01	8.86	14.51	0.53	0.17

Cases 2 and 3 modify the exterior temperature data and thus affect the heating demand of customers. In case 2 (case 3) where the exterior temperature is higher (lower) than case 0, the required heating demand is reduced (increased). Thus, the electricity procurement and daily energy costs of case 2 (case 3) are lower (higher) than case 0 as shown in Table V. In addition, the CHPs are able to consume more (less) gas to produce more (less) power and heat in case 2 (case 3) so that the household GFs are guaranteed to have sufficient fuel for heating.

C. Effectiveness of Reformulation Methods in Section III

The nonlinear constraints of the original MERS model in Section II is reformulated in Section III. To verify the effectiveness of the proposed reformulation methods, the performance of the following cases is simulated and the results compared in Table VI:

- Case 4: Base case setup with the original MERS model proposed in Section II. The MERS model is solved by the GAMS/BONMIN solver.
- Case 5: Base case setup with the original MERS model linearized by piecewise linearization methods described in the first paragraph of Section III. The linearized MILP model is solved by the GAMS/CPLEX solver.

As illustrated in Table VI, the daily energy cost of case 0 is significantly lower than that of case 4 and case 5. In fact, the solving of either case 4 or case 5 is terminated before reaching the optimum solution due to the execution time limit. Thus, the proposed reformulated model is superior to the complex MERS model and the piecewise linearization-based MILP model.

Although the MILP model in case 5 is feasible for linearizing the MERS model, the reformulations in [23] are designated for energy transmission systems and a large number of integer variables are employed, which significantly prolongs the solving time significantly. Take the test system in Fig. 2 as an example. The maximum number of binary variables of the proposed reformulated model and the piecewise linearization methods (with eight segments) in [23] are 15×96=1440 and (33+14)×8×96=36096, respectively. In addition, the direction of gas flow in a number of pipelines is known as a priori in most NGDSs. In Fig. 2, the gas flow direction in pipelines 14-3, 14-5, 14-8, 11-12, 1-13, and 13-5 is fixed, leaving only 9×96=864 binary variables. When dealing with larger energy distribution systems, the number of binary variables of the proposed reformulated model becomes much less than the MILP model that employs piecewise linearization. As a result, the proposed reformulated model has better performance and scalability for electric power and natural gas distribution networks.

TABLE VI
PERFORMANCE OF CASES 0, 4, AND 5

	Case 0	Case 4	Case 5
Daily energy cost ($)	2794.36	3674.32	2913.40
CPU time (s)	76.4	10000*	10000*

* Terminated due to execution time limit

Moreover, the accuracy of the proposed linearization methods in Section III is also investigated. The approximation of linepack proposed in (41) is very effective, with a maximum error of 0.02% compared with the accurate equation. Fig. 4 further compares the effectiveness of proposed approximation methods for compressor loss calculations. According to Fig. 4, the proposed approximation (46) performs much better than the widely used McCormick relaxation method. The average error and Euclidean distance from accurate loss are 0.0037 (m^3) and 0.0402 (m^3) based on proposed (46), and are –0.0177 (m^3) and 0.1972 (m^3) based on McCormick method, respectively. Besides, the approximation based on (46) tends to overestimate the compressor loss a little bit, which will lead to a conservative but robust compressor operating strategy. In summary, the proposed reformulation methods are able to relieve the computational burden and approximate the nonlinear equations and constraints with satisfactory accuracy at the same time.

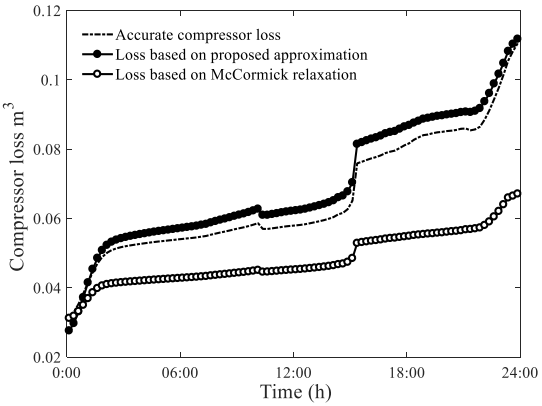

Fig. 4. Comparisons of compressor loss estimation with different methods.

D. Effectiveness of CCP Reformulation in Section IV

In Section IV, the linear reformulation of CCP is employed to handle the uncertainties introduced by RES generation, price fluctuation, etc. Table VII compares the optimization results based on the reformulated CCP and similar uncertainty modelling methods. Two comparative cases are defined as follows.

- Case 6: Base case setup solved by robust optimization method [42].
- Case 7: Base case setup while the $f^{-1}(1-\phi)$ in (69) is calculated based on the ICDF of the Gaussian distribution.

The comparisons among case 0, case 6, and case 7 are listed in Table VII. Compared to case 0, case 6 has a higher daily energy cost and lower RES generation output. Thus, the reformulated CCP with Chebyshev's inequality (case 0) leads to an operating strategy that is less conservative than case 6 that bases on robust optimization.

On the other hand, the daily energy cost and RES generation output of case 7 are lower and higher than that of case 0, respectively. However, the Gaussian distribution based case 7 tends to overestimate the RES generation capability and results

in constraint violations. The performances of (69) and Gaussian distribution based ICDF are further compared in Table VIII, where 10,000 data samples are generated for each considered distribution. Only the first and second moments of these random series are utilized by (69) and Gaussian distribution to estimate the possible derivations. In addition, real-world WPU and PVU generation data obtained from [41] are utilized to generate two more test cases:

- Case 8: Annual hourly data of two PVUs with a correlation coefficient of 0.975.
- Case 9: Case 8 plus an annual hourly WPU data series whose correlation coefficient with PVUs is –0.158.

Based on the confidence level and the first and second moments of the data, an estimation interval can be derived from either (69) or Gaussian distribution based ICDF. If the sampled data falls beyond the estimation interval, a *failure* is identified. In the case of MERS operation, a failure indicates the violation of a constraint. All failures are marked shaded in Table VIII. As can be seen from Table VIII, the performance of Gaussian distribution is acceptable when the uncertain factor follows lognormal distribution or Weibull distribution. For the uncertain factor that follows beta distribution or student's t distribution, Gaussian distribution is likely to underestimate the volatility of that factor and result in a higher failure rate. When dealing with correlated multiple data series in cases 11 and 12, the failure rates of Gaussian distribution based estimation increase dramatically. On the other hand, the failure rates of (69) based estimations are always kept within the confidence levels for both uncorrelated PDFs and correlated series obtained from real-world data. Thus, the adopted CCP reformulation with Chebyshev's inequality is distributionally robust and performs well dealing with correlated uncertain factors that widely exist in residential energy systems.

TABLE VII
COMPARISONS OF CASES 0, 6, AND 7

	Case 0	Case 6	Case 7
Daily energy cost ($)	2794.36	2857.87	2489.35
RES generation (MWh)	8.80	7.96	9.55

TABLE VIII
FAILURE RATE COMPARISON OF RES GENERATION ESTIMATION BASED ON CHEBYSHEV'S INEQUALITY AND GAUSSIAN DISTRIBUTION

Distribution (parameter)	Chebyshev's inequality		Gaussian distribution	
	ϕ =0.05	ϕ =0.01	ϕ =0.05	ϕ =0.01
Beta (2,1)	0.0%	0.0%	7.94%	1.50%
Lognormal (0.5,0.1)	0.0%	0.0%	3.96%	0.44%
Student's t (10)	0.06%	0.0%	4.47%	1.25%
Weibull (1,2)	0.0%	0.0%	1.62%	0.0%
Case 8	2.70%	0.09%	9.13%	6.53%
Case 9	1.24%	0.04%	24.32%	16.38%

In summary, Tables VII and VIII validate that the CCP based on Chebyshev's inequality is able to properly model the volatility of correlated random series while sacrificing a marginal amount of economic efficiency. For RESOs with insufficient generation data of RESs, the proposed distributionally robust model is the desirable solution to generate day-ahead operating schedules to avoid constraint violations that may subject to significant penalties in real-time energy markets.

VI. CONCLUSION

In this paper, a day-ahead optimal operation model of a MERS is established. The characteristics of different energy carriers are considered, and various types of RESs and DERs can be easily integrated into the developed model. The complex MERS model is properly reformulated and approximated as an MISOCP model. The uncertainties associated with RES generation forecast errors, load variations, and energy price fluctuations are modelled by a distributionally robust CCP reformulation technique. The effectiveness of the proposed reformulated model and the adopted distributionally robust CCP are validated through case studies. Compared to existing research, the proposed reformulated model is superior in modeling the MERSs and the uncertainty associated with the generation outputs of correlated RESs. Moreover, the proposed reformulated model offers great benefits to RESOs as it is less conservative than the conventional robust optimization and very effective in managing risks associated with issues such as constraint violations.

APPENDIX

A. AC Power Flow of a PDS

The AC power flow for a PDS is usually described by the following equations and constraints:

$$P_{n,t} = P_{n,t}^{G} - P_{n,t}^{D} = \sum_{m\in\Omega_N} P_{n-m,t} \tag{A1}$$

$$Q_{n,t} = Q_{n,t}^{G} - Q_{n,t}^{D} = \sum_{m\in\Omega_N} Q_{n-m,t} \tag{A2}$$

$$P_{n-m,t} = V_{n,t}V_{m,t}(G_{n-m}\cos(\theta_{n,t}-\theta_{m,t}) + B_{n-m}\sin(\theta_{n,t}-\theta_{m,t})) \tag{A3}$$

$$Q_{n-m,t} = V_{n,t}V_{m,t}(G_{n-m}\sin(\theta_{n,t}-\theta_{m,t}) - B_{n-m}\cos(\theta_{n,t}-\theta_{m,t})) \tag{A4}$$

$$P_{n,t}^{\min} \le P_{n,t} \le P_{n,t}^{\max} \tag{A5}$$

$$Q_{n,t}^{\min} \le Q_{n,t} \le Q_{n,t}^{\max} \tag{A6}$$

$$V_{n}^{\min} \le V_{n,t} \le V_{n}^{\max} \tag{A7}$$

$$-I_{n-m}^{\max} \le I_{n-m,t} \le I_{n-m}^{\max} \tag{A8}$$

where (A1) and (A2) calculate the nodal active/reactive power injections, (A3) and (A4) calculate the branch power flows, and (A5)-(A8) constrain active and reactive power injection, nodal voltage magnitudes, and line current magnitudes, respectively. In Section II.B, (A1)-(A4) and (A5)-(A8) are represented by (2) and (3), respectively.

B. SOCP Relaxation for a Radial PDS

For a radial PDS, the nonlinear AC power flow (A1)-(A8) can be effectively relaxed to an SOCP problem by replacing the original variables $V_{n,t}$ and $\theta_{n,t}$ with three sets of new variables described in (A9)-(A11), respectively, and a conic constraint described in (A12) [34]. By relaxing (A1)-(A8) with the SOCP technique, the new set of variables in the relaxed PDS operation model is denoted as $\mathbf{X}_1^*$, where $\mathbf{X}_1^* = \{P_{n,t}, Q_{n,t}, U_{n,t}, R_{n-m,t}, K_{n-m,t}\}$.

$$U_{n,t} = (V_{n,t})^2 \tag{A9}$$

$$R_{n-m,t} = V_{n,t}V_{m,t}\cos(\theta_{n,t}-\theta_{m,t}) \tag{A10}$$

$$K_{n-m,t} = V_{n,t}V_{m,t}\sin(\theta_{n,t}-\theta_{m,t}) \tag{A11}$$

$$U_{n,t}U_{m,t} \ge (R_{n-m,t})^2 + (K_{n-m,t})^2 \tag{A12}$$

As a result, (A3) and (A4) can be reformulated as (A13) and (A14), respectively.

$$P_{n-m,t} = g_{n-m}U_{n,t} - g_{n-m}R_{n-m,t} - b_{n-m}K_{n-m,t} \tag{A13}$$

$$Q_{n-m,t} = -(b_{n-m} + b_{n-m}^{sh}/2)U_{n,t} + b_{n-m}R_{n-m,t} - g_{n-m}H_{n-m,t} \tag{A14}$$

where g_{n-m}, b_{n-m}, and b_{n-m}^{sh} are the series conductance, series susceptance, and shunt susceptance in the π-model of distribution line *n-m*, respectively.

To calculate the magnitudes of nodal voltage and line current using $\mathbf{X}_1^*$, (A7) and (A8) should be reformulated as (A15) and (A16)-(A17), respectively.

$$(V_{n}^{\min})^2 \le (V_{n,t})^2 \le (V_{n}^{\max})^2 \tag{A15}$$

$$(I_{n-m,t})^2 \le (I_{n-m}^{\max})^2 \tag{A16}$$

$$(I_{n-m,t})^2 = (g_{n-m}^2 + (b_{n-m} + b_{n,m}^{sh}/2)^2)U_{n,t} + (g_{n-m}^2 + b_{n-m}^2)U_{m,t} - (2g_{n-m}^2 + 2b_{n-m}^2 + b_{n-m}b_{n-m}^{sh})R_{n-m,t} + g_{n-m}b_{n-m}^{sh}K_{n-m,t} \quad \text{(A17)}$$

REFERENCES

[1] A. Ipakchi and F. Albuyeh, "Grid of the future," *IEEE Power & Energy Mag.*, vol. 7, no. 9, pp. 52-62, Mar. 2009.

[2] W. A. Bukhsh, C. Zhang, and P. Pinson, "An integrated multiperiod OPF model with demand response and renewable generation uncertainty," *IEEE Trans. Smart Grid*, vol. 7, no. 3, pp. 1495-1053, May 2016.

[3] A. Q. Huang, M. L. Crow, G. T. Heydt, J. P. Zheng, and S. J. Dale, "The future renewable electric energy delivery and management (FREEDM) system: the energy internet," *Proc. IEEE*, vol. 99, no. 1, pp. 133-148, Jan. 2011.

[4] M. Geidl and G. Andersson, "Optimal power flow of multiple energy carriers," *IEEE Trans. Power Syst.*, vol. 22, no. 1, pp. 145-155, Feb. 2007.

[5] P. Duenas, T. Leung, M. Gil, and J. Reneses, "Gas-electricity coordination in competitive markets under renewable energy uncertainty," *IEEE Trans. Power Syst.*, vol. 30, no. 1, pp. 123-131, Jan. 2015.

[6] E. Dall'Anese, P. Mancarella, and A. Monti, "Unlocking flexibility: integrated optimization and control of multienergy systems," *IEEE Power & Energy Mag.*, vol. 15, no. 1, pp. 43-52, Feb. 2017.

[7] W. Su, J. Wang, and J. Roh, "Stochastic energy scheduling in microgrids with intermittent renewable energy resources," *IEEE Trans. Smart Grid*, vol. 5, no. 4, pp. 1876-1883, Jul. 2014.

[8] J. Qiu, Z. Y. Dong, J. H. Zhao, K. Meng, Y. Zheng, and D. J. Hill, "Low carbon oriented expansion planning of integrated gas and power systems," *IEEE Trans. Power Syst.*, vol. 30, no. 2, pp. 1035-1046, Mar. 2015.

[9] X. Zhang, M. Shahidehpour, A. Alabdulwahab, and A. Abusorrah, "Optimal expansion planning of energy hub with multiple energy infrastructures," *IEEE Trans. Smart Grid*, vol. 6, no. 5, pp. 2302-2311, Sep. 2015.

[10] M. Geidl, G. Koeppel, P. Favre-Perrod, B. Klockl, G. Andersson, and K. Frohlich, "Energy hubs for the future," *IEEE Power & Energy Mag.*, vol. 5, no. 1, pp. 24-30, Mar. 2007.

[11] M. Moeini-Aghtaie, A. Abbaspour, M. Fotuhi-Firuzabad, and E. Hajipour, "A decomposed solution to multiple-energy carriers optimal power flow," *IEEE Trans. Power Syst.*, vol. 29, no. 2, pp. 707-716, Mar. 2014.

[12] Y. Wen, X. Qu, W. Li, X. Liu, and X. Ye, "Synergistic operation of electricity and natural gas networks via ADMM," *IEEE Trans. Smart Grid*, early access, 2017.

[13] C. M. Correa-Posada and P. Sanchez-Martin, "Security-constrained optimal power and natural gas flow," *IEEE Trans. Power Syst.*, vol. 29, no. 4, pp. 1780-1787, Jul. 2014.

[14] M. Qadrdan, J. Wu, N. Jenkins, and J. Ekanayake, "Operating strategies for a GB integrated gas and electricity network considering the uncertainty in wind power forecasts," *IEEE Trans. Sustain. Energy*, vol. 5, no. 1, pp. 128-138, Jan. 2014.

[15] C. He, L. Wu, T. Liu, and M. Shahidehpour, "Robust co-optimization scheduling of electricity and natural gas systems via ADMM," *IEEE Trans. Sustain. Energy*, vol. 8, no. 2, pp. 658-670, Apr. 2017.

[16] S. Clegg and P. Mancarella, "Integrated electrical and gas network flexibility assessment in low-carbon multi-energy systems," *IEEE Trans. Sustain. Energy*, vol. 7, no. 2, pp. 718-731, Apr. 2016.

[17] Z. Qiao, Q. Guo, H. Sun, Z. Pan, Y. Liu, and W. Xiong, "An interval gas flow analysis in natural gas and electricity coupled networks considering the uncertainty of wind power," *Applied Energy*, vol. 201, pp. 343-353, Sep. 2017.

[18] M. C. Bozchalui, S. A. Hashmi, H. Hassen, C. A. Canizares, and K. Bhattacharya, "Optimal operation of residential energy hubs in smart grid," *IEEE Trans. Smart Grid*, vol. 3, no. 4, pp. 1755-1766, Dec. 2012.

[19] A. Anvari-Moghaddam, J. M. Guerrero, J. C. Vasquez, H. Monsef, and A. Rahimi-Kian, "Efficient energy management for a grid-tied residential microgrid," *IET Gener. Transm. Distrib*., vol. 11, no. 11, pp. 2752-2761, Aug. 2017.

[20] H. Karami, M. J. Sanjari, S. H. Hosseinian, and G. B. Gharehpetian, "An optimal dispatch algorithm for managing residential distributed energy resources," *IEEE Trans. Smart Grid*, vol. 5, no. 5, pp. 2360-2367, Sep. 2014.

[21] M. Rastegar, M. Fotuhi-Firuzabad, H. Zareipour, and M. Moeini-Aghtaie, "A probabilistic energy management scheme for renewable-based residential energy hubs," *IEEE Trans. Smart Grid*, vol. 8, no. 5, pp. 2217-2227, Sep. 2017.

[22] H. Wu, A. Pratt, and S. Chakraborty, "Stochastic optimal scheduling of residential appliances with renewable energy sources," in *IEEE PES General Meeting*, Denver, CO, USA, Jul. 2015.

[23] C. Shao, X. Wang, M. Shahidehpour, X. Wang, and B. Wang, "An MILP-based optimal power flow in multicarrier energy system," *IEEE Trans. Sustain. Energy*, vol. 8, no. 1, pp. 239-248, Jan. 2017.

[24] X. Zhang, M. Shahidehpour, A. Alabdulwahab, and A. Abusorrah, "Hourly electricity demand response in the stochastic day-ahead scheduling of coordinated electricity and natural gas networks," *IEEE Trans. Power Syst.*, vol. 31, no. 1, pp. 592-601, Jan. 2016.

[25] N. Good and P. Mancarella, "Flexibility in multi-energy communities with electrical and thermal storage: a stochastic, robust approach for multi-service demand response," *IEEE Trans. Smart Grid*, early access, 2017.

[26] L. Ni, W. Liu, F. Wen, Y. Xue, Z. Dong, Y. Zheng, and R. Zhang, "Optimal operation of electricity, natural gas and heat systems considering integrated demand responses and diversified storage devices," *J. Mod. Power Syst. Clean Energy*, vol. 6, no. 3, pp. 423-437, May 2018.

[27] Natural Resources Canada's Office of Energy Efficiency, "Survey of household energy use detailed statistical report," 2011 [Online]. Available:https://oee.nrcan.gc.ca/publications/statistics/sheu/2011/pdf/sheu2011.pdf

[28] P. M. Coelho and C. Pinho, "Considerations about equations for steady state flow in natural gas pipelines," *J. Braz. Soc. Mech. Sci. Eng.*, vol. 29, no. 3, pp. 262-273, Jul. 2007.

[29] M. Chaudry, N. Jenkins, and G. Strbac, "Multi-time period combined gas and electricity network optimisation," *Electr. Power Syst. Res.*, vol. 78, no. 7, pp. 1265-1279, Jul. 2008.

[30] Y. Dai, L. Chen, Y. Min, Q. Chen, K. Hu, J. Hao, Y. Zhang, and F. Xu, "Dispatch model of combined heat and power plant considering heat transfer process," *IEEE Trans. Sustain. Energy*, vol. 8, no. 3, pp. 1225-1236, Jul. 2017.

[31] F. Salgado and P. Pedrero, "Short-term operation planning on cogeneration systems: a survey," *Electr. Power Syst. Res.*, vol. 78, no. 5, pp. 835-848, May 2008.

[32] X. Chen, C. Kang, M. O'Malley, Q. Xia, J. Bai, C. Liu, R. Sun, W. Wang, and H. Li, "Increasing the flexibility of combined heat and power for wind power integration in China: modeling and implication," *IEEE Trans. Power Syst.*, vol. 30, no. 4, pp. 1848-1857, Jul. 2015.

[33] W. Liu, Q. Wu, F. Wen, and J. Østergaard, "Day-ahead congestion management in distribution systems through household demand response and distribution congestion prices," *IEEE Trans. Smart Grid*, vol. 5, no. 6, pp. 2739-2747, Nov. 2014.

[34] H. Zhang, V. Vittal, G. T. Heydt, and J. Quintero, "A relaxed AC optimal power flow model based on a Taylor series," in *IEEE Innovative Smart Grid Technologies-Asia*, Bangalore, India, Nov. 2013.

[35] N. C. Koutsoukis, D. O. Siagkas, P. S. Georgilakis, and N. D. Hatziargyriou, "Online reconfiguration of active distribution networks for maximum integration of distributed generation," *IEEE Trans. Autom. Sci. Eng.*, vol. 14, no. 2, pp. 437-448, Apr. 2017.

[36] R. A. Jabr, R. Singh, and B. C. Pal, "Minimum loss network reconfiguration using mixed-integer convex programming," *IEEE Trans. Power Syst*., vol. 27, no. 2, pp. 1106-1115, May 2012.

[37] L. Roald and G. Andersson, "Chance-constrained AC optimal power flow: reformulations and efficient algorithms," *IEEE Trans. Power Syst.*, early access, 2017.

[38] H. Qu, L. Roald, and G. Andersson, "Uncertainty margins for probabilistic AC security assessment," in *Proc. IEEE Eindhoven Powertech*, Eindhoven, Netherlands, Jun. 2015.

[39] J. Schmidli, L. Roald, S. Chatzivasileiadis, and G. Andersson, "Stochastic AC optimal power flow with approximate chance-constraints," in *IEEE PES General Meeting*, Boston, MA, USA, Jul. 2016.

[40] Y. Zhang, S. Shen, and J. L. Mathieu, "Distributionally robust chance-constrained optimal power flow with uncertain renewables and uncertain reserves provided by loads," *IEEE Trans. Power Syst.*, vol. 32, no. 2, pp. 1378-1388, Mar. 2017.

[41] Natural Resources Canada, "Renewables," [Online]. Available: http://www.nrcan.gc.ca/energy/renewable-electricity/7293

[42] D. Bertsimas and M. Sim, "The price of robustness," *Oper. Res.*, vol. 52, no. 1, pp. 35-53, Feb. 2004.

Weijia Liu received the B.Eng. and Ph.D. degrees in electrical engineering from Zhejiang University, Hangzhou, China, in 2011 and 2016, respectively.

He is currently a Postdoctoral Fellow in the Department of Electrical and Computer Engineering, University of Saskatchewan, Saskatoon, SK, Canada.

His research interests include the integrated energy systems, smart grid, power system restoration, and electricity market.

Junpeng Zhan (M'16) received the B.Eng. and Ph.D. degrees in electrical engineering from Zhejiang University, Hangzhou, China, in 2009 and 2014, respectively.

He is currently a Research Associate Electrical Engineer in the Sustainable Energy Technologies Department, Brookhaven National Laboratory, Upton, NY, USA. He was a Postdoctoral Fellow in the Department of Electrical and Computer Engineering, University of Saskatchewan, Saskatoon, SK, Canada.

His research interests include the integration of renewable electric energy sources, energy storage systems, and dynamic thermal rating into power systems.

C. Y. Chung (M'01-SM'07-F'16) received the B.Eng. (with First Class Honors) and Ph.D. degrees in electrical engineering from The Hong Kong Polytechnic University, Hong Kong, China, in 1995 and 1999, respectively.

He is currently a Professor, the NSERC/SaskPower (Senior) Industrial Research Chair in Smart Grid Technologies, and the SaskPower Chair in Power Systems Engineering in the Department of Electrical and Computer Engineering at the University of Saskatchewan, Saskatoon, SK, Canada.

Dr. Chung is an Editor of *IEEE Transactions on Power Systems* and *IEEE Transactions on Sustainable Energy* and an Associate Editor of *IET Generation, Transmission, & Distribution*. He is also an IEEE PES Distinguished Lecturer and a Member-at-Large (Global Outreach) of the IEEE PES Governing Board.

Yang Li received the B.Eng. degree in electrical engineering from Zhejiang University, Hangzhou, China, in 2014.

He is currently pursuing the Ph.D. degree in the College of Electrical Engineering, Zhejiang University, Hangzhou, China.

His research interests include the integrated energy systems and power system optimization.